Novel Hybrid Analytical/Numerical Conducted EMI Model of a Flyback Converter

Weichang Cheng, Zhi Huang, Shen Xu, and Weifeng Sun, *Senior Member, IEEE*

***Abstract*—A hybrid analytical/numerical conducted an electromagnetic interference (EMI) modeling approach, which adopts both numerical method and analytical method, is proposed in this paper. In this model, the noise source is calculated directly with the original data from oscilloscopes. The noise path at different operating status is extracted from the original converter topology and its analytical expression is then derived. Also, according to the EMI receiver detector mode, the algorithm of the EMI receiver is proposed in this paper. Peak (PK), average (AV), and quasi-peak (QP) values of the EMI can then be calculated to analyze the impact of each relevant component. The analytical method is provided to carry out PK, AV, and QP simulations accurately and fast. The simulation and experimental results for common mode leakage currents validate this EMI model. Furthermore, two analysis examples are given to illustrate how this model is applied for engineers.**

***Index Terms*—AC–DC power conversion, electromagnetic conductive interference, modeling.**

I. Introduction

OWING to high efficiency and wide range of voltage converting, the flyback converters are widely used in low-power consumer electronics. However, the high-frequency switching actions of MOSFET in the flyback converters cause serious electromagnetic interference (EMI) problems. EMI noise has the potential to interfere with the system operation [1]. Since 1990s, the power converters are compelled to comply with the stringent electromagnetic-compatibility (EMC) regulations and standards before being released to the consumer market. Thus, it is necessary to find out the EMI characteristics of the flyback converters. Understanding and characterizing the complex EMI phenomena through accurate modeling and prediction of EMI-noise propagation are necessary prerequisites for solving the EMI problem effectively. In order to predict conducted EMI noise, the conducted EMI model has to be established.

Modeling the propagation path is significant and often challenging. Many papers have discussed and proposed modeling approaches for the noise path. In [2]–[6], lumped circuit models to build the whole system model in circuit simulation software such as Pspice or Saber have been used. The parasitic parameters of components are calculated from the impedance test result. Lumped circuit models allow engineers to analyze the impact of each component. However, such models are often too complex for practical use and the complexity of the simulation circuit usually causes some nonconvergence problem in the circuit simulation software. In [7]–[9], terminal modeling, classified as the behavioral modeling techniques, is employed in power converters and three-phase ac systems. An estimation of the ports network model of noise sources and paths is required, which is obtained by measurement [8]. Behavioral models are easy to build and theoretically precise if the accuracy of the impedance test equipment is high. However, the impact of each parameter on EMI cannot be observed in this type of model as it is limited to showing the final result rather than revealing the EMI mechanism.

Peak (PK), average (AV), and quasipeak (QP) are the three separate testing modes of EMI. As the impacts of component on these three different testing modes are very different, it is necessary to include the EMI receiver into the simulation model. Algorithms for PK, AV, and QP models are presented only in a few literatures [10]–[15]. However, the methods of calculating QP values are computer resource consuming and some algorithms are only appropriate for a certain kind of converters.

In this paper, a novel method of the EMI noise is proposed. In our model, the components' impedances and noise source directly employ the original testing data to improve the accuracy and simplify the modeling procedure. Based on modeling the propagation path, analytical expression for conducted EMI noise is then derived. Depending on the mechanism of the PK, AV, and QP detectors, a simplified EMI receiver model is also proposed. Taken together, a hybrid analytical/numerical (HAN) algorithm for conducted EMI simulation is proposed. A flyback converter is then modeled adopting this method as an example. The newly developed model achieves good accuracy, which is compatible with the analysis and the model developed in this work. By adopting both analytical and numerical algorithms, this model achieves greater accuracy and less complexity than lumped circuit model. Furthermore, this approach allows engineers to analyze the effect of each component on conducted EMI or diagnosing their printed circuit board (PCB) designs.

II. Principle of Conducted EMI Test

In this section, a brief introduction of the principle of the conducted EMI measurement is given in order to algorithmize the EMI test system. Fig. 1 shows a general simplified model of the EMI noise propagation along with the test equipment. Before it is finally measured, the noise signal passes through three devices, which are the equipment under test (EUT), line impedance stabilization network (LISN), and EMI receiver. EMI noise is generated from the power converter and then propagated

Manuscript received May 11, 2016; revised July 15, 2016 and September 6, 2016; accepted September 12, 2016. Date of publication October 4, 2016; date of current version December 6, 2016. This work was supported by the National Nature Science Foundation of China (61674033), the Natural Science Foundation of the Jiangsu Province (BK20161148) and Qing Lan Project.

The authors are with the National ASIC System Engineering Research Center, Southeast University, Nanjing 210096, China (e-mail: swffrog@seu.edu.cn).

Color versions of one or more of the figures in this paper are available online at http://ieeexplore.ieee.org.

Digital Object Identifier 10.1109/TEMC.2016.2610467

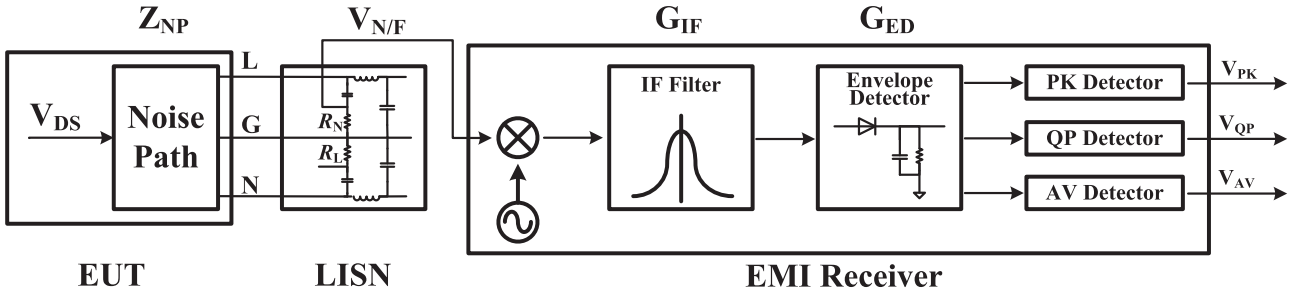

Fig. 1. Simplified model of EMI test.

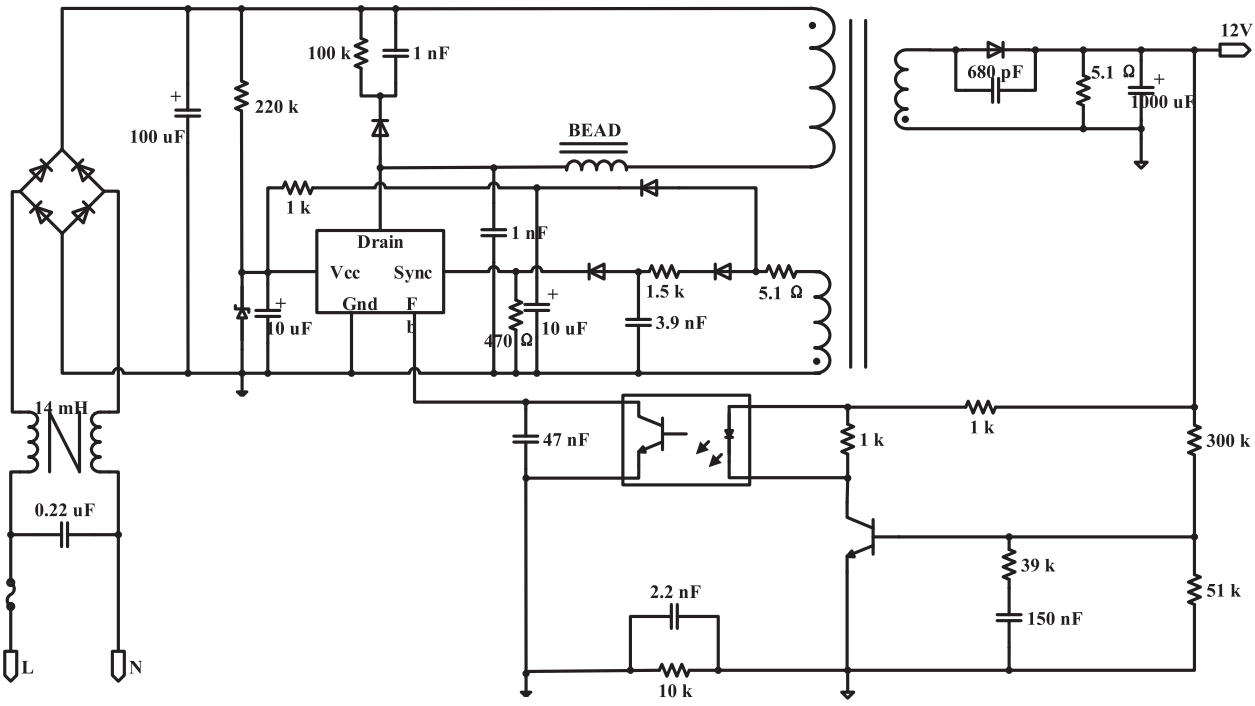

Fig. 2. Illustration of the flyback converter.

to LISN. LISN is a filter to isolate the noise from the power grid; thus, the EMI receiver only receives the noise from the EUT. An EMI receiver is composed of a mixer, an intermediate frequency (IF) filter, an envelope detector, and three different detectors. When the noise reaches the EMI receiver, it will be shifted to the center frequency of the IF filter. Along with the envelope detector, the IF filter outputs the envelope of the noise at a certain frequency. Finally, the noise is sent to PK, QP, and AV detector to evaluate separately. Obviously, the algorithmization of noise path and EMI receiver is the prerequisite of achieving a precise and analyzable conducted EMI model.

III. Conducted EMI Modeling of a Flyback Converter

In this section, the principles of the conducted EMI modeling which are applied on a conventional flyback converter are introduced. Noise source, propagation path, and EMI receiver are modeled separately and then combined as the complete EMI model of a flyback converter. The circuit diagram of this flyback converter and the values of components are all shown in Fig. 2.

A. Noise Source

Abrupt changes in current or voltage generate high-frequency harmonics [16]. Those high-frequency harmonics ranging from 150 kHz to 30 MHz will be measured by an EMI receiver as conducted EMI. In flyback converters, fast switching actions of power MOSFET are the major noise source of EMI [16]. The voltage waveform between the Drain pin (which is connected to the drain of MOSFET) and GND pin (which is connected to the source of MOSFET) is shown in Fig. 3. Three different high-frequency components can be identified in the $V_{\rm ds}$ pin voltage. The switching frequency, which is the most prominent frequency because of its large amplitude [17], is generated by the switching of the MOSFET. This frequency component is usually between 10 and 300 kHz in ac–dc power converters. The other two are generated by the resonances in each cycle as shown in Fig. 3 [18]. The frequency of the first resonance which is caused by the leakage inductance (transformer) and parasitic capacitance (transformer and MOSFET) is usually between 1 and 10 MHz. The frequency of the second resonance which is caused by the magnetizing inductance (transformer) and parasitic capacitance (transformer

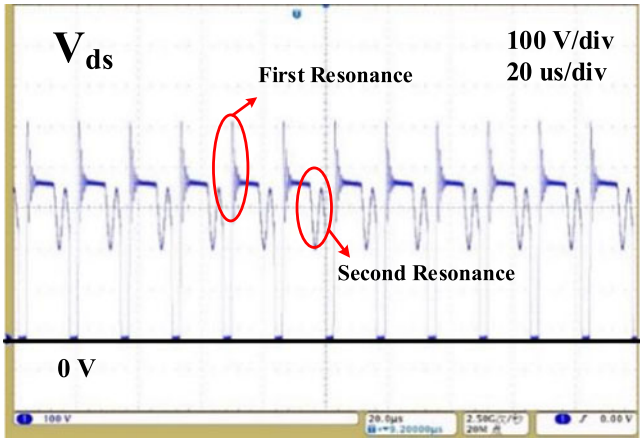

Fig. 3. Waveform of the voltage of the Drain pin.

and MOSFET) is usually between 200 kHz and 1 MHz. Furthermore, the voltage waveform on secondary winding also contains high-frequency components. While, as its amplitude is only a seventh of the amplitude of $V_{\rm ds}$ in this case, these frequencies can thus be neglected. The noise source is mostly modeled as a simple pulse waveform in the former models [2]–[9]. Therefore, only switching frequency is considered into the modeling. In the model presented in this paper, the noise source is measured by an oscilloscope and the original measured data are taken into the calculation directly. Thus, the influences of two other resonance frequencies are also reflected in the final simulation result.

B. Modeling of Common Mode (CM) Noise Paths

Conducted EMI can be divided into differential mode (DM) EMI and CM EMI. The generation mechanisms and noise propagation paths of these two types of EMI noise are different [16]. DM currents flow out of the live wire and return via the neutral wire. CM currents take the live and neutral wires as one outgoing conductor and return via the ground wire [19]. The equivalent circuit of conducted EMI, which is composed of relevant components, parasitic parameters, and LISN, is built to analyze EMI noise propagation paths.

Relevant components are first modeled including the passive and active components. Passive components show different behaviors at high frequencies because of the parasitic effect. The frequency response characteristic of impedance can be measured by an impedance analyzer. The original data are directly applied in the presented model in this paper without building the high-frequency model. Therefore, the passive component can be easily and precisely modeled. What calls for a special attention is that both CM and DM impedances for the CM choke are required. Those can be measured with the two windings of the CM choke connected in series and in parallel [20]. The models of the active components used in this paper are shown in Table I. $C_{d1}-C_{d4}$, the value of which is decided by the type of the diode, which are junction capacitance of the rectifier diodes. According to the datasheet, the value is 30 pF. $C_{\rm ds}$ is equivalent capacitance between drain and source of a MOSFET. $C_{\rm ds}$ varies with the change of $V_{\rm ds}$. Under normal operation, $V_{\rm ds}$ in this flyback converter is either 0 V (when the MOSFET is ON) or above 200 V (when the MOSFET is OFF). $C_{\rm ds}$ maintains around 100 pF when $V_{\rm ds}$ is above 200 V.$C_{\rm ds}$ can be simply regarded as a 100 pF capacitor when the MOSFET is OFF. When $V_{\rm ds}$ is 0 V (the MOSFET is ON), $C_{\rm ds}$ is shorted and the value does not need to be considered.

TABLE I
MODELS OF THE ACTIVE COMPONENTS

Components	Models
Rectifier Bridge	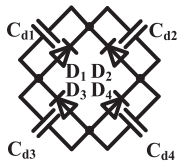
MOSFET	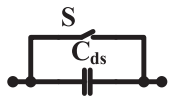

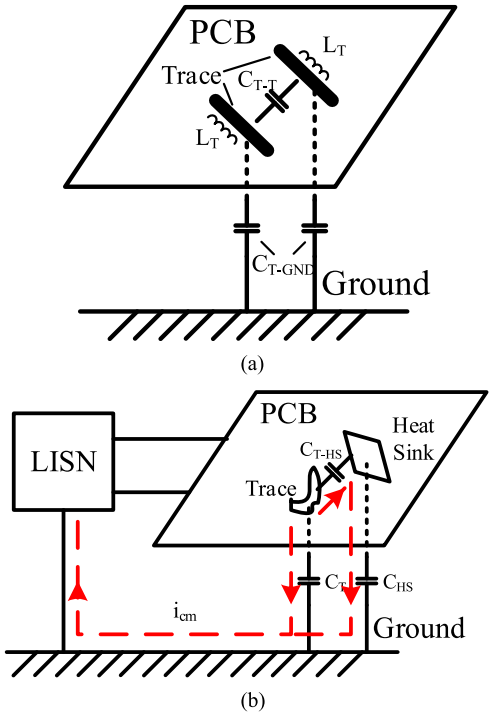

Fig. 4. Parasitic effect in PCB (a) parasitic parameters and (b) components of $C_{\rm gnd}$.

PCB is also very relevant to EMI through the parasitic parameters. Three kinds of parasitic parameters can be identified in PCB as shown in Fig. 4(a): the parasitic inductance L_T; the coupling capacitance between traces and ground ($C_{\rm T-GND}$); and the coupling capacitance between traces (C_{T-T}). L_T is first neglected as it is connected to the circuit in series and is usually very small. $C_{\rm T-GND}$ is a primary CM noise path. C_{T-T} may cause crosstalk between traces. These two parameters are mainly determined by the area of the traces. However, the frequency range of conducted EMI is only up to 30 MHz. Only

TABLE II
Q3D SIMULATION RESULT

C_T/pF	C_{T-HS}/pF	C_{HS}/pF
0.15945	0.21501	2.2887

when the amplitude of the high-frequency signal of traces is high enough ("hot node"), those parameters are unneglectable. In this case, the trace on the noise source is considered as noise source is the only "hot node." Also, heat sink is another crucial part because it is usually designed as a large area to achieve enough heat dissipation and it is extremely close to the noise source. In our paper, the parasitic parameters of these two parts are equivalent to a capacitor $C_{\rm gnd}$. The visualized noise path is shown in Fig. 4(b). $C_{T-\rm HS}$ represents the capacitance between the trace of the noise source and heat sink. C_T is the capacitance between the noise source trace and the ground. $C_{\rm HS}$ is the capacitance between the heat sink and ground. Therefore, $C_{\rm gnd}$ can be calculated as

$$C_{\rm gnd} = \frac{1}{\frac{1}{C_{\rm HS}} + \frac{1}{C_{T-\rm HS}}} + C_T. \tag{1}$$

All these capacitances are modeled and simulated by Q3D, the simulation result is listed in Table II.

Then the equivalent circuits of CM and DM propagation paths, which are shown in Fig. 5(a) and (c), are derived separately; since, the generation mechanisms and noise propagation of CM EMI and DM EMI are different [16]. As discussed before, the Drain pin is the noise source, which is equivalent to a voltage source in a noise propagation model. The CM noise path is marked as a solid line and the DM noise is marked as a dashed line. Thus, the noise path model of CM and DM EMI noises can be extracted separately as shown in Fig. 5(b) and (d).

EMI noise paths are different under different operating conditions of the system. In consideration of the OFF--ON state of MOSFET and rectifier diodes, there are four states for CM EMI and DM EMI separately. Extractions of CM EMI models are demonstrated here as examples.

1) CM noise when mosfet and a pair of diodes are both on: The rectifier diodes turn ON only when the input capacitor $C_{\rm in}$ is charging. The CM EMI noise path at this status is shown in Fig. 5(a). Nodal analysis is applied to analyze, since, the leg number of circuit is big and the node point number is small in this case. Applying Kirchhoff's law and Ohm's law at each node, the nodal circuit equation is expressed as follows:

$$\begin{cases} \left(\frac{1}{Z_{\rm in}} + \frac{1}{Z_{\rm rcd}} + \frac{1}{Z_{\rm bt}} + \frac{1}{Z_{\rm lc}}\right) \cdot U_1 = \frac{1}{Z_{\rm lc}} \cdot U_2 \\ \frac{1}{Z_{\rm lc}} \cdot U_1 + \frac{1}{Z_x} \cdot U_3 + \frac{1}{Z} \cdot U_4 = \left(\frac{1}{Z_{lc}} + \frac{1}{Z_x} + \frac{1}{Z}\right) \cdot U_2 \\ \frac{1}{Z_{\rm lc}} + \frac{1}{Z_x} + \frac{1}{r} \cdot U_3 = \frac{1}{Z_x} \cdot U_2 + \frac{1}{Z} \cdot U_4 \\ \frac{1}{Z} \cdot (U_2 + U_3) + \frac{V_{ds}(f)}{Z_{\rm gnd}} = \left(\frac{2}{Z} + \frac{1}{Z_{\rm gnd}}\right) \cdot U_4. \end{cases} \tag{2}$$

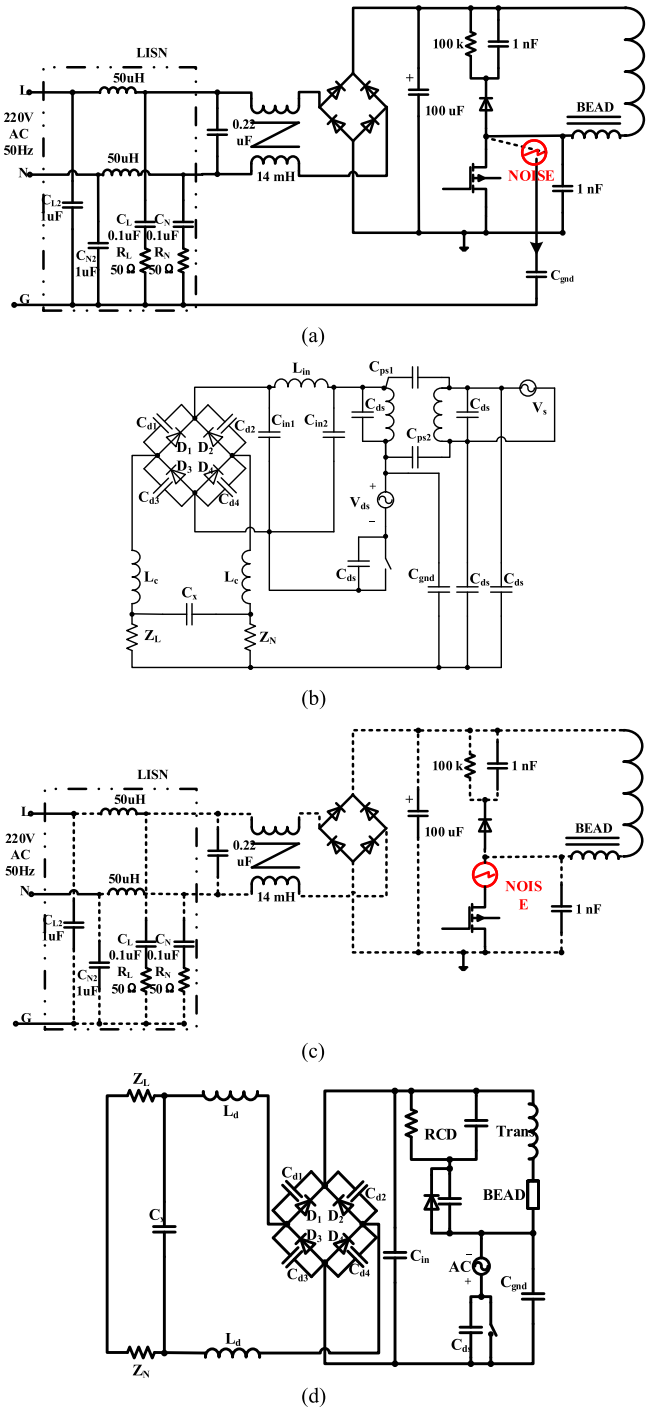

Fig. 5. Equivalent circuit of CM and DM noise paths (a) CM noise path of the flyback converter. (b) Equivalent circuit of CM noise path. (c) DM noise path of the flyback converter. (d) Equivalent circuit of DM noise path.

As a matter of convenience in algorithmization, (2) is then transformed to matrix form as follows:

$$A \cdot \begin{bmatrix} U_1 \\ U_2 \\ U_3 \\ U_4 \end{bmatrix} = \begin{bmatrix} 0 \\ 0 \\ 0 \\ -\frac{V_{\rm ds}(f)}{Z_{\rm gnd}} \end{bmatrix} \tag{3}$$

where Eq.(4) shown at the bottom of this page.

$$Z_{\rm bt} = Z_{\rm trans} + Z_{\rm BEAD} \tag{5}$$

$$Z = \left(50 + \frac{1}{j \cdot 2\pi \cdot f \cdot 0.1\mu{\rm F}}\right) // \left(j \cdot 2\pi \cdot f \cdot 50\mu{\rm H} + \frac{1}{j \cdot 2\pi \cdot f \cdot 1\mu{\rm F}}\right). \tag{6}$$

$Z_{\rm in}$ is the impedance of $C_{\rm in}$. $Z_{\rm rcd}$ is the impedance of RCD snubber. $Z_{\rm bt}$, which follows (5), is the sum of $Z_{\rm Trans}$ (impedance of the transformer original side) and $Z_{\rm BEAD}$ (impedance of the bead). $Z_{\rm lc}$ is the impedance of CM model of the CM choke. Z_x is the impedance of C_x and Z is the impedance of two branches (Z_L and Z_N) in the LISN as shown in (6). $Z_{\rm gnd}$ is the impedance of $C_{\rm gnd}$. Worth to note that, $V_{\rm ds}(f)$ is the voltage of the EMI noise source at any test frequency, which can be obtained by a Fourier transform of the noise source signal.

Thus, the voltage on R_N in LISN can be calculated from the values of the nodal voltages as

$$V_{N|{\rm CM1}}(f) = \frac{50}{Z} \cdot (U_4 - U_3) = \frac{50}{Z} \cdot \left(\begin{bmatrix} 0 & 0 & -1 & 1 \end{bmatrix} \cdot A^{-1} \cdot \begin{bmatrix} 0 \\ 0 \\ 0 \\ -\dfrac{V_{\rm ds}(f)}{Z_{\rm gnd}} \end{bmatrix} \right) \tag{7}$$

(7) can be simplified as

$$V_{N|{\rm CM1}}(f) = H_{N|{\rm CM1}}(f) \cdot V_{\rm ds}(f). \tag{8}$$

2) CM noise when mosfet is off and one pair of diodes is on: As shown in Fig. 6(b), when the MOSFET turns OFF, noise current flows through $C_{\rm ds}$ and the bypass capacitor C of the MOSFET. With the same method, we can obtain both $H_{N|{\rm CM2}}$ and $V_{N|{\rm CM2}}$.

3) CM noise mosfet is off and diodes are off: When the voltage on $C_{\rm in}$ is higher than the voltage of input, rectifier diodes are OFF. Therefore, the CM current can only flow through the junction capacitance of the rectifier diodes. The noise path at this occasion is shown in Fig. 6(c).

4) CM noise mosfet is on and diodes are off: Following the method depicted in 1), we can obtain the CM voltage on R_N under this circumstance as shown in Fig. 6(d).

C. Modeling of DM Noise Paths

When one pair of diodes is ON, the voltage on R_N for DM EMI which is shown in (9) and (10) can be derived from the DM equivalent circuit illustrated in Fig. 5(d) in the same way. $V_{N|{\rm DM1}}$ and $V_{N|{\rm DM2}}$ represent the DM noise voltage on R_N when the MOSFET is OFF and ON separately

$$V_{N|{\rm DM1}}(f) = \frac{V(f)}{2} \times \frac{50}{Z} \times \frac{2Z//Z_x}{2Z//Z_x + 2Z_{\rm ld}} \times \frac{(2Z//Z_x + 2Z_{\rm ld})//Z_{\rm in}}{(2Z//Z_x + 2Z_{\rm ld})//Z_{\rm in} + Z_{\rm rcd1}//Z_{\rm bt}} \times \frac{((2Z//Z_x + 2Z_{\rm ld})//Z_{\rm in} + Z_{\rm rcd1}//Z_{\rm bt})//Z_c}{((2Z//Z_x + 2Z_{\rm ld})//Z_{\rm in} + Z_{\rm rcd1}//Z_{\rm bt})//Z_c + Z_{\rm ds}} \tag{9}$$

$$V_{N|{\rm DM2}}(f) = \frac{V(f)}{2} \times \frac{50}{Z} \times \frac{2Z//Z_x}{2Z//Z_x + 2Z_{\rm ld}} \times \frac{(2Z//Z_x + 2Z_{\rm ld})//Z_{\rm in}}{(2Z//Z_x + 2Z_{\rm ld})//Z_{\rm in} + Z_{\rm rcd2}//Z_{\rm bt}} \tag{10}$$

$Z_{\rm ld}$ is the impedance of DM model of the CM choke.

When rectifier diodes are all OFF, the calculation of the voltage on R_N is briefer. A simplified model of LISN at this status is shown in Fig. 7. $Z_{\rm lf}$ is the impedance of LISN and filter sets (*X* capacitor and common mode choke in this system). Since the diodes used in the rectifier are the same and the junction capacitance of a diode is only decided by its type, $C_{\rm d1} - C_{\rm d4}$ are supposed to have the same impedance value. Based on the principle of Wheatstone bridge, $V_{\rm CD}$ is zero and no current flows through LISN when all rectifier diodes turn OFF. In other words, $V_{N|{\rm DM3}} = V_{N|{\rm DM4}} = 0$.

D. Voltage on Z_N and Z_L

To calculate the frequency spectrum of EMI noise, the waveform of voltage on R_N and R_L of at least one line cycle should be acquired. Here, we also take R_N as an example. V_N is the sum of $V_{N|{\rm CM}}$ and $V_{N|{\rm DM}}$, according to the definition of conducted EMI. Based on the conclusion in the last segment, the voltage on R_N or R_L at each status can be calculated. Thus, V_N can be acquired by combining the waveform at different status correspondingly. It is worth noting that the directions of DM currents are contrary when different pairs of diodes are ON as shown in Fig. 8. As V_N equals to the sum of CM and DM noises, it is divided into six statuses. When the system is in the normal operation, noise source can be approximated to a periodic waveform

$$A = \begin{bmatrix} \dfrac{1}{Z_{\rm in}} + \dfrac{1}{Z_{\rm rcd2}} + \dfrac{1}{Z_{\rm bt}} + \dfrac{1}{Z_{\rm lc}} & -\dfrac{1}{Z_{\rm lc}} & 0 & 0 \\ \dfrac{1}{Z_{\rm lc}} & -\dfrac{1}{Z_{\rm lc}} - \dfrac{1}{Z_x} - \dfrac{1}{Z} & \dfrac{1}{Z_x} & \dfrac{1}{Z} \\ 0 & -\dfrac{1}{Z_x} & \dfrac{1}{Z_{\rm lc}} + \dfrac{1}{Z_x} + \dfrac{1}{r} & -\dfrac{1}{Z} \\ 0 & \frac{1}{Z} & \frac{1}{Z} & -\frac{2}{Z} - \frac{1}{Z_{\rm gnd}} \end{bmatrix} \tag{4}$$

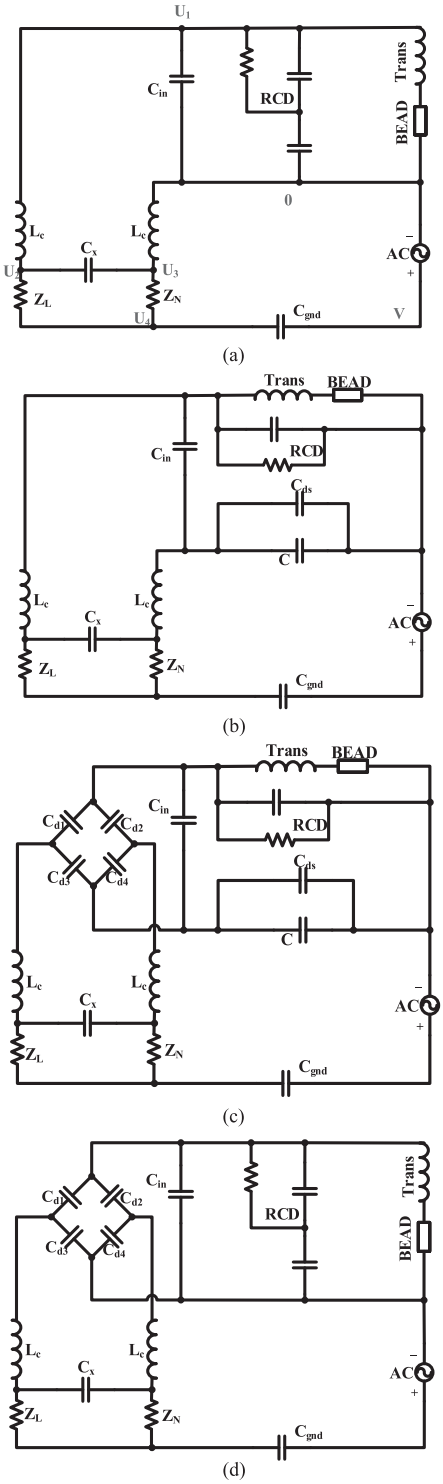

Fig. 6. CM EMI noise path in those three occasions (a) when the MOSFET is ON and the diodes are ON, (b) when the MOSFET is OFF and the diodes are ON, (c) when the MOSFET is OFF and the diodes are OFF, and (d) when the MOSFET is ON and the diodes are OFF.

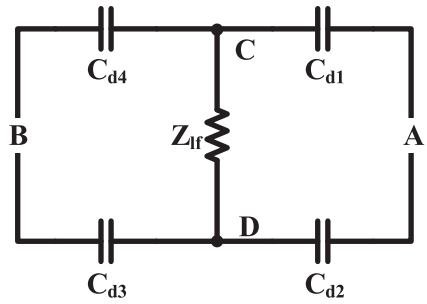

Fig. 7. Preceding stage circuit when rectifier diodes turn OFF.

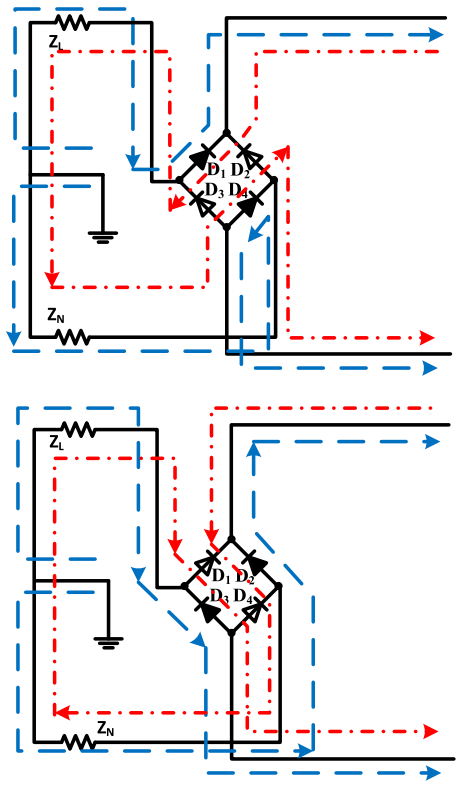

Fig. 8. Directions of noise current when different pairs are ON, blue dashed line for CM path red dash-dot line for DM path (a) when D_1 and D_4 are ON and (b) when D_2 and D_3 are ON.

TABLE III
TRANSFER FUNCTIONS IN DIFFERENT STATUSES

CM transfer function	DM transfer function	Status
$H_{N\|CM1}(f)$	$H_{N\|DM1}(f)$	MOSFET-on | D1, D3-on
$H_{N\|CM2}(f)$	$H_{N\|DM2}(f)$	MOSFET-off | D1, D3-on
$H_{N\|CM1}(f)$	$-H_{N\|DM1}(f)$	MOSFET-on | D2, D4-on
$H_{N\|CM2}(f)$	$-H_{N\|DM2}(f)$	MOSFET-off | D2, D4-on
$H_{N\|CM3}(f)$	0	MOSFET-off | D1, D3 or D2, D4-on
$H_{N\|CM4}(f)$	0	MOSFET-on | D1, D3 or D2, D4-on

and the turn-on time of rectifier diodes or MOSFET is constant. The CM and DM transfer functions in different statuses are listed in Table III. The period of each state can be derived by the duty ratio of the rectifier diodes and MOSFET. At 220-V ac input and full load, D_d and DM are measured as 6.9% and 16.1% separately. $H_{N|CM1}$, $H_{N|CM2}$, $H_{N|CM3}$, $H_{N|CM4}$, $H_{N|DM1}$, and $H_{N|DM2}$ represent the CM and DM transfer functions in different states, respectively. Those transfer functions can be obtained by applying the method introduced above. $V_N(t)$ then is sent to the EMI receiver to calculate the EMI noise.

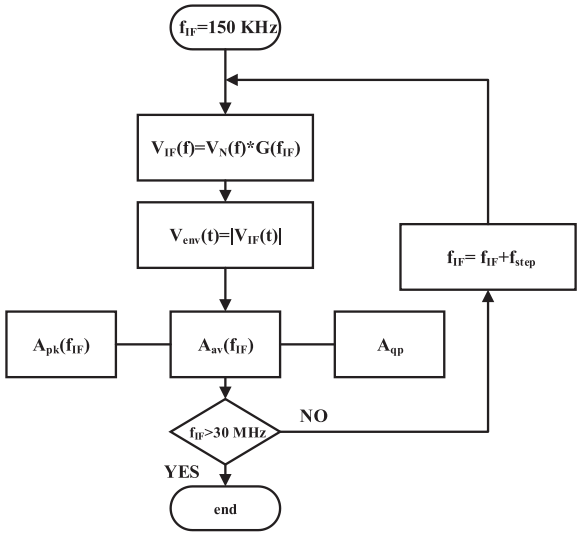

Fig. 9. Flowchart of EMI measurement.

E. EMI Receiver

EMI receiver processes the voltage data from LISN and outputs EMI spectrum. The simplified model consists of a mixer, a local oscillator, an IF filter, an envelope detector, and EMI detectors. EMI receivers have to fulfill the requirements that are given by the international standard CISPR16-1-1 [21]. As specified in CISPR-16-1-1, the IF is a band-pass filter with a 9-kHz resolution bandwidth at -6 dB. Associated with the mixer and the local oscillator, the IF filter can be modeled as an IF filter with a tunable center frequency. The amplitude gain of the equivalent IF filter is expressed as in the following equation [15], where f_{IF} is the center frequency of the IF filter

$$|G_{\mathrm{IF}}(f)| = e^{-\left[\frac{(f-f_{\mathrm{IF}})\sqrt{\ln 2}}{4.5\cdot 10^3}\right]^2}. \tag{11}$$

The envelope detector detects the envelope of the noise filtered through the IF filter. At last, the noise signal is sent to the EMI detectors, which output the PK, QP, and AV values. The EMI receiver is a stepwise instrument. The flowchart is shown in Fig. 9. The center frequency of IF filter (f_{IF}) moves by steps within the frequency range from 150 kHz to 30 MHz to separate the EMI noise around each specified frequency. Then, those noise data are sent to EMI detectors.

Fig. 10 shows the different outputs that the same noise signal passes through PK, QP, and AV detectors separately. The PK and AV values are maximum and average values of the envelope signal separately as expressed below

$$A_{\mathrm{MAX}}|_f = \mathrm{MAX}[V(t)|_f] \tag{12}$$

$$A_{\mathrm{AV}}|_f = \mathrm{MEAN}[V(t)|_f]. \tag{13}$$

The QP detector consists of charging and discharging networks and a critically damped meter, they are connected by a buffer to avoid any repercussion. According to [11], for proper QP detection, a duration time of at least 2 s is required to achieve a steady state at each frequency point. Obviously, long-duration

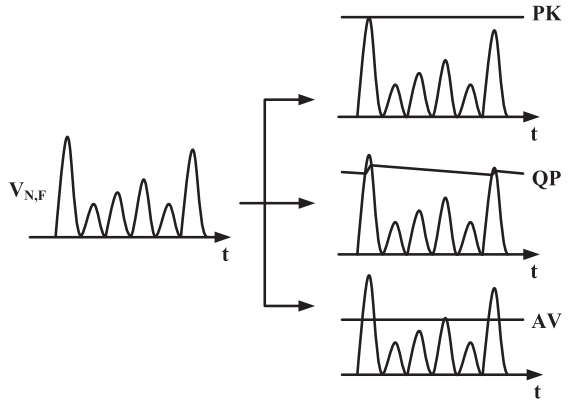

Fig. 10. Simplified model of an EMI receiver.

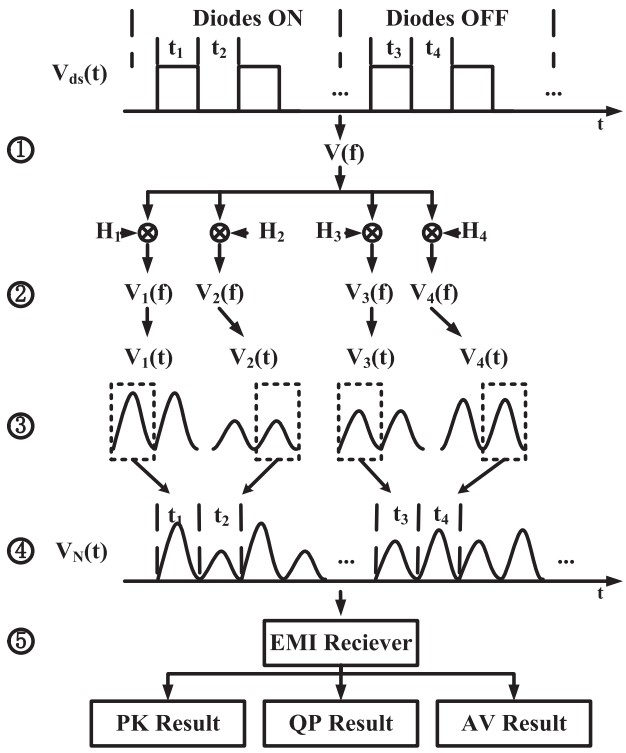

Fig. 11. Illustration of the procedure to calculate $V_N(f)$.

calculation time lowers the simulation efficiency and also consumes vast computer resources when conducting QP simulation on the computer. However, the output of the critically damped meter is in proportion to the periodic input. As a result, the average value of the output of the charging and discharging networks, which is the input signal of the critically damped meter, is used as the approximation of the QP value. With this method, the time and computer memory needed for the critically damped meter are both reduced. Thus, the proposed QP algorithm is more suitable for predicting QP value of the conducted EMI.

F. Algorithmization

The procedures to calculate the final EMI simulation result as shown in Fig. 11 can be described as follows:

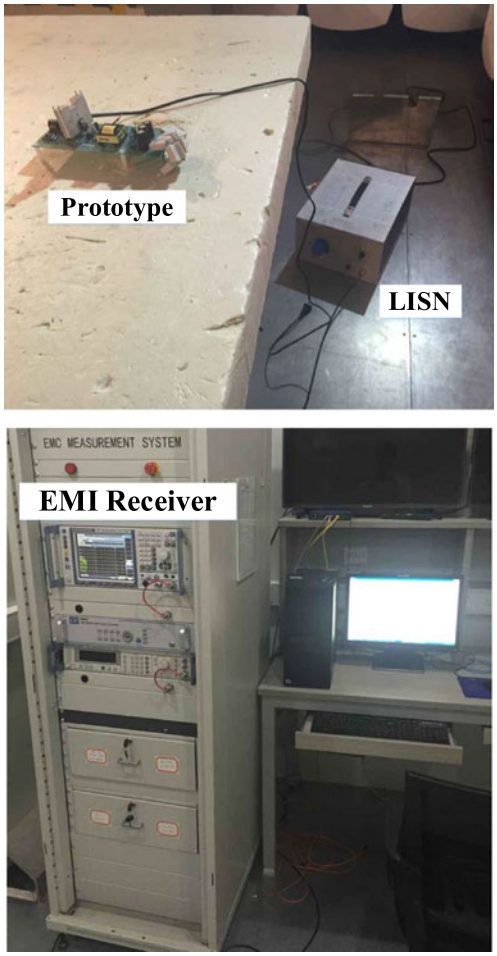

Fig. 12. Arrangement and apparatus of conducted EMI measurement.

1) The transfer function *H*(*f*) is a frequency related function, $V_{\mathrm{ds}}(t)$ is first transformed to the frequency domain by using the Fast Fourier Transform.
2) Calculate $V_1(f), V_2(f), \ldots, V_4(f)$. $V_n(f) = V_{\mathrm{ds}}(f) \cdot H_n(f)$, where $n = 1, 2, \ldots, 6$. $V_n(f)$ and $H_n(f)$ represent the CM/DM voltage of R_N and the CM/DM transfer function, respectively. $V_{\mathrm{ds}}(f)$ is the complete spectrum of $V_{\mathrm{ds}}(t)$ in a full time range. In this algorithm, the switching action is not included as the frequencies of falling and rising edges are too high (above 15 MHz, will be above 30 MHz in future miniaturized power converter). Practically, the lower frequency is the key range that EMI problems mostly occur (the second and third harmonics of switching frequency). Therefore, we took the approximation that the switching action is simply divided to on- and off-state by the threshold of MOSFET.
3) Convert $V_1(f)$, $V_2(f), \ldots, V_4(f)$ to the time domain by using an Inverse Fast Fourier Transform.
4) The final $V_{N|CM}(t)$ and $V_{N|DM}(t)$ are constructed by picking the corresponding time "pieces" from the individual $V_n(t)$. The sum of them is the final EMI noise $V_N(t)$. It is worth noting that when different pair of diodes are ON, the direction of DM current flow though sampling resistant is different. Therefore, as shown in Table III, there are six different combinations of CM and DM noises.

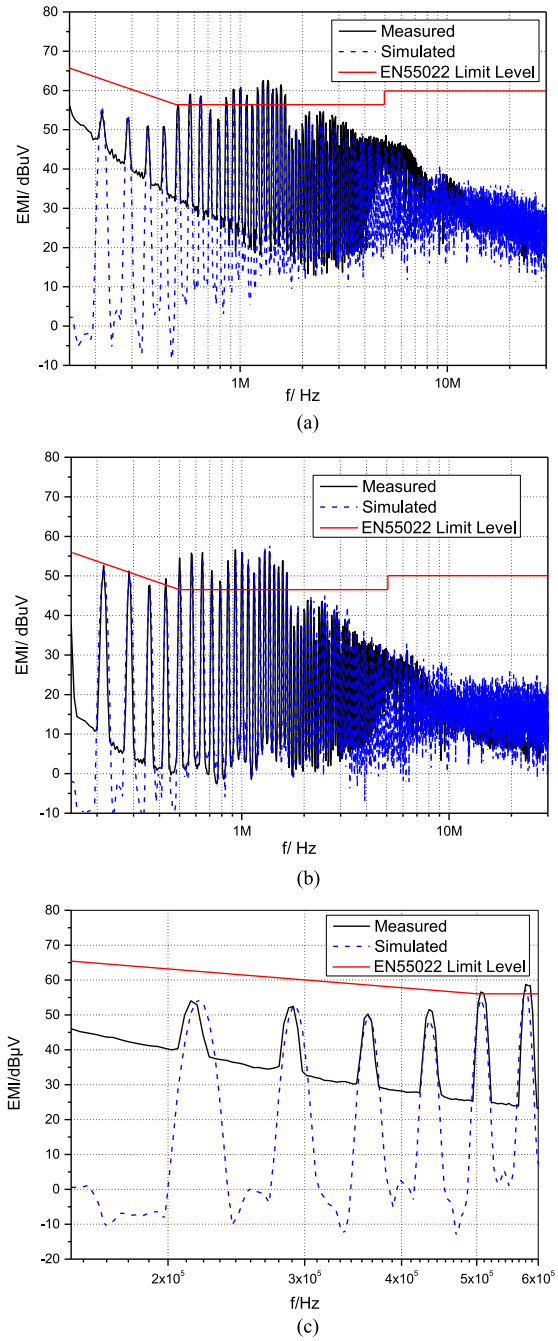

Fig. 13. Comparison between measured and predicted PK, AV, and QP values of conducted EMI (a) PK values of conducted EMI, (b) AV values of conducted EMI, and (c) QP values of conducted EMI.

5) Send $V_N(t)$ to the EMI receiver calculation program and obtain the final result.

IV. Validation

Given an ac input voltage of 220 V, a frequency of 50 Hz, and the load of the 40 W, the CM EMI test is launched. The measurement setup is shown in Fig. 12.

The comparison of PK, AV, and QP values of conducted EMI shows that the newly developed model works well. Since QP test time is extremely time consuming, only a part of data (under 0.6 MHz) is measured to verify the accuracy of the

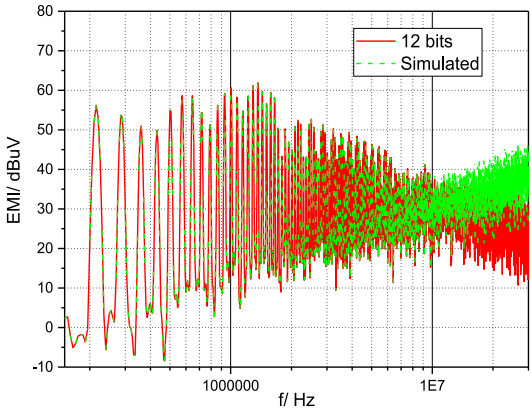

Fig. 14. Simulation results of different original noise source data.

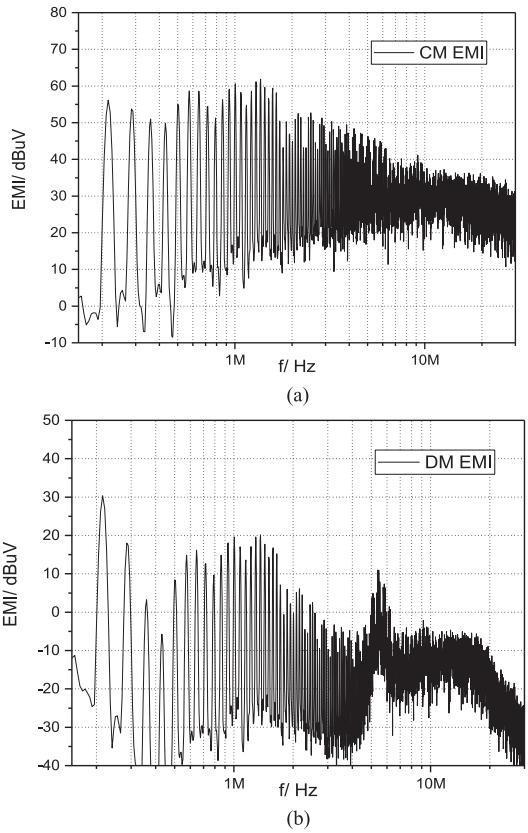

Fig. 15. Simulated and measured impacts of C_{gnd} (a) simulated impacts in full frequency range and (b) measured impact of PK value.

model. In Fig. 13(a)–(c), small difference is observed below 3 dBμV from 150 kHz to 10 MHz. The accuracy at the frequency range from 10 to 30 MHz drops as the analog-digital converter (ADC) of the oscilloscope brings high-frequency noise. With a more precise oscilloscope, the accuracy can be boosted further, especially at high frequency [9]. Even though, the accuracy of lumped parameter model is acceptable for engineers to predict conducted EMI in power converters.

It is worth mentioning that the measurement accuracy of $V_{\mathrm{ds}}(t)$ affects the simulation result remarkably at high frequency. A LeCroy ZS1000 active probe is employed to measure V_{ds}. The input capacitor of the probe is connected to the MOSFET in parallel (0.9 pF according to the datasheet). As the C_{ds} is usually about 20–200 pF (100 pF in this case) at a high voltage, the impact of C_{probe} can be neglected. The number of bits of ADC in the oscilloscope should be high enough as low-resolution measurement may bring in some unwanted high-frequency noise. As shown in Fig. 14, larger error can be observed in the final simulation results by employing the data measured by an 8 bits oscilloscope.

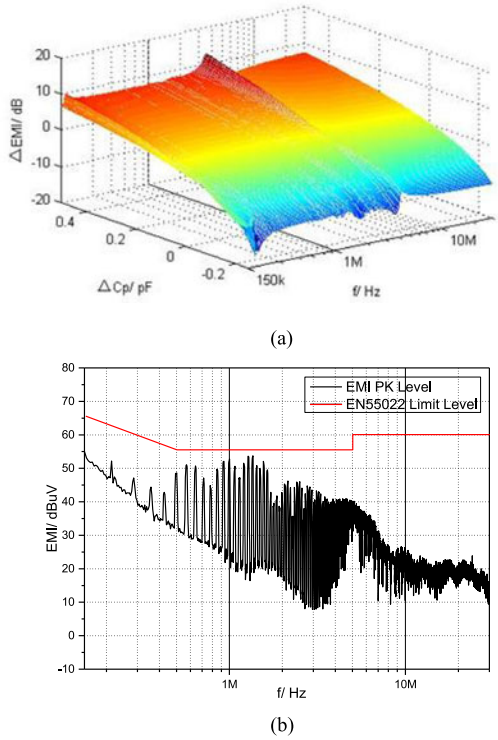

Fig. 16. Simulated and measured impacts of C_{gnd} (a) simulated impacts in full frequency range and (b) measured PK value of optimized converter.

While this model achieves good accuracy, the reductions of simulation time consuming and computer resource consuming are remarkable. Only relative component is required to be modeled. Thus, compared to the lumped circuit models, this model is easier and more efficient to construct.

Another advantage of this model is that both CM and DM EMI can be simulated separately. Therefore, targeted solutions can be put out to solve EMI problem of different patterns. As a conclusion, this model can be a helpful tool for the engineers when dealing with the EMI problem. As shown in Fig. 15, the CM noise is considerably larger than the DM noise. Thus, if only DM countermeasure is made, the EMI noise cannot be suppressed.

By adopting this model, the impact of each parameter can be shown visually to the engineer. As the CM noise is the dominated pattern in this case, here, we take C_{gnd} as an example. Fig. 16(a) shows the impact on EMI when increased by 0.4 pF to be decreased by 0.2. *Z*-axis represents the variation of EMI, *Y*-axis is the variation of the C_{gnd}, and *x*-axis represents the frequency. It can be observed that the EMI is related to the C_{gnd} positively in full frequency range. By decreasing the size of the heat sink, 10 dB declines of the EMI measurement result can be observed in Fig. 16(b).

V. Conclusion

In this paper, an accurate EMI modeling approach is proposed. The model presented in this paper combines the lumped circuit model and the behavioral model. The noise path is extracted to avoid the extensive calculation of the lumped circuit model. Unlike the former two types of models, noise source and components are modeled separately by employing the testing data directly to balance the simplicity and the analyzability of the EMI models. A HAN algorithm is developed to solve the different operating status problems. According to the mechanism of the PK, AV, and QP detectors, a simplified EMI receiver model is also proposed. This HAN model is easier to construct than the lumped models and allows researchers to better understand the impact of each parameter than the behavioral model. By this model, PK, AV, and QP values of EMI can all be simulated accurately. The maximum difference between the measurement and the predicted results is below 3 dBμV at most part of the frequency range.

References

[1] L. Premalatha, T. A. Raghavendiran, and C. Ravichandran, "Experimental study on conducted EMI mitigation in SMPS using a novel spread spectrum technique," *J. Power Electron.*, vol. 13, no. 4, pp. 619–625, Jul. 2013.

[2] R. Y. Mohammad, A. F. Nahid, and F. Jawad, "Conducted electromagnetic interference evaluation of forward converter with symmetric topology and passive filter," *IET Power Electron.*, vol. 7, no. 5, pp. 1113–1120, 2014

[3] Q. D. Wang, Z. Y. An, Y. L. Zheng, and Y. M. Yang, "Parameter extraction of conducted electromagnetic interference prediction model and optimization design for a DC-DC converter system," *IET Power Electron.*, vol. 6, no. 7, pp. 1449–1461, 2013.

[4] J.-L. Kotny, X. Margueron, and N. Idir, "High frequency modeling method of EMI filters," in *Proc. Energy Convers. Congr. Expo.*, 2009, pp. 1671–1678

[5] J. Sun and L. Xing, "Parameterization of three-phase electric machine models for EMI simulation," *IEEE Trans. Power Electron.*, vol. 29, no. 1, pp. 36–41, Jan. 2014.

[6] S. Manivannan, R. Arumugam, S. Paramasivam, P. Salil, and B. S. Rao, "HFSS simulation, experimental investigation and optimisation of heat sink EMI," *IET Power Electron.*, vol. 3, no. 6, pp. 881–891, 2010

[7] A. C. Baisden, P. Mattavelli, and D. Boroyevich, "Analysis of EMI terminal modeling of switched power converters," *IEEE Trans. Power Electron.*, vol. 27, no. 9, pp. 3924–3933, Sep. 2012.

[8] A. C. Baisden, D. Boroyevich, and F. Wang, "Generalized terminal modeling of electromagnetic interference," *IEEE Trans. Ind. Appl.*, vol. 46, no. 5, pp. 2068–2079, Sep./Oct. 2010.

[9] J. S. Wei, D. Gerling, and M. Gelek, "Experimental characterization of conducted EMI in three-phase power electronics system using terminal model," in *Proc. Int. Symp. Power Electron. Electr. Drivers Autom. Motion*, 2014, pp. 1184–1189.

[10] F. Krug, S. Braun, and P. Russer, "A novel quasi-peak-detector for time-domain EMI-measurements," *Adv. Radio Sci.*, vol. 2, pp. 27–32, 2004.

[11] F. Krug, S. Braun, Y. Kishida, and P. Russer, "A novel digital quasi-peak detector for time-domain measurements," in *Proc. 33rd Eur. Microw. Conf.*, 2003, pp. 1027–1030

[12] Z. J. Wang, S. Wang, P. J. Kong, and F. C. Lee, "DM EMI noise prediction for constant on-time, critical mode power factor correction converters," *IEEE Trans. Power Electron.*, vol. 27, no. 7, pp. 3150–3157, Jul. 2012.

[13] S. Braun, T. Donauer, and P. Russer, "A real-time time-domain EMI measurement system for full-compliance measurements according to CISPR 16-1-1," *IEEE Trans. Electromagn. Compat.*, vol. 50, no. 2, pp. 259–26, May 2008

[14] T. Nussbaumer, M. L. Heldwein, and J. W. Kolar, "Differential mode input filter design for a three-phase buck-type PWM rectifier based on modeling of the EMC test receiver," *IEEE Trans. Ind. Electron.*, vol. 53, no. 5, pp. 1649–1661, Oct. 2006

[15] Q. Ji, X. B. Ruan, and Z. H. Ye, "The worst conducted EMI spectrum of critical conducntioon mode boost PFC converter," *IEEE Trans. Power Electron.*, vol. 30, no. 3, pp. 1230–1241, Mar. 2015

[16] M. R. Yazdani, H. Farzanehfard, and J. Faiz, "Classification and comparison of EMI mitigation techniques in switching power converters—A review," *J. Power Electron.*, vol. 11, no. 5, pp. 767–777, 2011.

[17] W. C. Cheng, X. Y. He, S. Xu, and W. F. Sun, "Analysis of common-mode electromagnetic interference noise in a flyback converter using a self-supply power control integrated circuit," *IET Power Electron.*, vol. 8, no. 9, pp. 1749–1757, 2015.

[18] A. I. Pressman, K. Billings, and T. Morey, *Switching Power Supply Design*, 3rd ed. New York, NY, USA: McGraw-Hill, 2008.

[19] K. Y. See, "Network for conducted EMI diagnosis," *Electron. Lett.*, vol. 35, no. 17, pp. 1446–1447, Aug. 1999.

[20] H. L. Chen and Z. M. Qian, "Modeling and characterization of parasitic inductive coupling effects on differential-mode EMI performance of a boost converter," *IEEE Trans. Electromagn. Compat.*, vol. 53, no. 4, pp. 1072–1080, Nov. 2011.

[21] *Specification for Radio Disturbance and Immunity Measuring Apparatus and Methods Part 1-1: Radio Disturbance and Immunity Measuring Apparatus—Measuring Apparatus, International Electrotechnical Commission CISPR 16-1-1*, Switzerland, 2006.

Weichang Cheng received the B.S. and M.S. degrees both in electronics engineering from the Southeast University, in 2006 and 2010, respectively. He is currently working toward the Ph.D. degree in electronics engineering at Southeast University, School of Electronic Science & Engineering.

His research interests include EMC and SI in power electronics.

Zhi Huang received the B.S. and M.S. degrees both in electronics engineering from the Southeast University, Nanjing, China, in 2013 and 2016, respectively.

Her research interests include EMC in power electronics.

Shen Xu received the B.S. and Ph.D. degrees both in electronics engineering from Southeast University, Nanjing, China, in 2002 and 2011, respectively.

He joined the School of Electronic Science and Engineering, Southeast University, Nanjing, China, in 2011, where he is currently an Associate Professor. His research interests include nonlinear modeling of power converters, simulations, and power integration.

Weifeng Sun (SM'13) was born in Jiangsu province, China, in 1977. He received the B.S., M.S., and Ph.D. degrees all in electronic engineering from the Southeast University, Nanjing, China, in 2000, 2003, and 2007, respectively.

He is currently the Dean in the School of Electronic Science & Engineering, Southeast University, China. His research interests mainly include new power device, power IC, power device model, power system, and reliability. He has authored 120 Chinese patents and has authored or co-authored more than 100 papers.